

Tracing Back the Malicious Clients in Poisoning Attacks to Federated Learning

Yuqi Jia
Duke University
yuqi.jia@duke.edu

Minghong Fang
Duke University
minghong.fang@duke.edu

Hongbin Liu
Duke University
hongbin.liu@duke.edu

Jinghuai Zhang
University of California, Los Angeles
jinghuai1998@g.ucla.edu

Neil Zhenqiang Gong
Duke University
neil.gong@duke.edu

Abstract

Poisoning attacks compromise the training phase of federated learning (FL) such that the learned global model misclassifies attacker-chosen inputs called *target inputs*. Existing defenses mainly focus on protecting the training phase of FL such that the learnt global model is poison free. However, these defenses often achieve limited effectiveness when the clients’ local training data is highly non-iid or the number of malicious clients is large, as confirmed in our experiments. In this work, we propose *FLForensics*, the first *poison-forensics* method for FL. *FLForensics* complements existing training-phase defenses. In particular, when training-phase defenses fail and a poisoned global model is deployed, *FLForensics* aims to trace back the malicious clients that performed the poisoning attack after a misclassified target input is identified. We theoretically show that *FLForensics* can accurately distinguish between benign and malicious clients under a formal definition of poisoning attack. Moreover, we empirically show the effectiveness of *FLForensics* at tracing back both existing and adaptive poisoning attacks on five benchmark datasets.

1 Introduction

Federated learning (FL) [1] is a distributed learning paradigm, allowing multiple clients to collaboratively train a model (called *global model*) under the coordination of a server without exposing their individual training data to the server. In essence, the FL training process is iterative. Specifically, each training round of FL entails the following: the server sends the current global model to all participating clients or a selected subset of them. These clients, using the received global model and their private training data, update their *local models*, and then send their model updates to the server. Subsequently, the server aggregates these model updates and further updates the global model. FL has been widely deployed in various real-world applications, such as credit risk prediction [2] and next-word prediction [3].

However, FL is vulnerable to poisoning attacks due to its distributed nature. An attacker can compromise training phase of FL via sending carefully crafted model updates from *malicious clients* to the server [4–6]. The poisoned global model misclassifies an attacker-chosen input (called *target input*) as an attacker-chosen label (called *target label*), but its classification accuracy for non-target inputs is unaffected. A target input can be *any* input embedded with an attacker-chosen trigger (these attacks are known as backdoor attacks) or a clean input without a trigger.

Existing defenses against poisoning attacks to FL mainly focus on *protecting the training phase*. For instance, many studies proposed robust FL methods (e.g., [7–10]) to prevent malicious clients from poisoning a global model. Specifically, a robust FL method—such as Trim [7], Median [7], FLTrust [9], and FLAME [8]—uses a robust aggregation rule to filter potentially malicious model updates when aggregating clients’ model updates. Other studies [11] proposed methods to detect malicious clients during training. For instance, FLDetector [11] detects the clients whose model updates are inconsistent across multiple training rounds as malicious. However, these training-phase defenses are insufficient. In particular, they achieve limited effectiveness when the clients’ local training data is highly non-iid or the number of malicious clients is large, as shown in our experiments. This is because it is hard to distinguish between

malicious clients’ model updates and benign clients’ ones in such scenarios. As a result, even if these training-phase defenses are adopted, the learnt global model may still be poisoned and the poisoned global model is deployed.

Our work: In this work, we propose *FLForensics*, the first *poison-forensics* method for FL. FLForensics complements training-phase defenses and they can be used together in a defense-in-depth fashion. Forensics in cybersecurity generally refers to analyzing the root cause of an attack after it has happened. In the context of FL, our FLForensics aims to trace back the malicious clients that performed the poisoning attack after the attack has happened, i.e., after training-phase defenses fail, a poisoned global model has been deployed, and a misclassified target input has been identified. We note that identifying a misclassified target input after model deployment is orthogonal to FLForensics, and can be achieved via manual inspection or automatic detection [12–14]. For instance, we show that our FLForensics can be adapted to detect whether a misclassified input is a misclassified target input or not in Section 8. FLForensics consists of two major steps: *calculating influence scores* and *detecting malicious clients*. The first step aims to calculate an influence score for each client based on its influence on the given misclassification of the target input; and the second step distinguishes between malicious clients and benign ones.

Calculating influence scores. One challenge to calculate clients’ influence scores is how to quantify the misclassification of a target input. To address the challenge, we use the cross-entropy loss of the global model for the misclassified target input. Moreover, since a client influences a global model and thus the cross-entropy loss through multiple training rounds, we expand the training rounds to calculate clients’ influence scores. Another challenge is that clients’ local training data are often non-iid. Specifically, some benign clients (denoted as *Category I*) have a large amount of local training examples with the target label, while other benign clients (denoted as *Category II*) do not. As a result, both malicious clients and Category I benign clients have large influence scores, making it challenging to distinguish them. To address this challenge, we propose that the server uses another *non-target input* with the target label to compute another influence score for each client. The server can simply generate a random input as the non-target input and assign the target label to it when calculating its cross-entropy loss. Thus, each client i has a two-dimensional influence score (s_i, s'_i) , which are obtained using the target input and non-target input, respectively.

Detecting malicious clients. We observe that malicious clients have large influence scores s_i but small s'_i ; Category I benign clients have large both s_i and s'_i ; and Category II benign clients have small both s_i and s'_i . Based on such observations, we propose a clustering-based method to detect malicious clients. We first use HDBSCAN [15] to divide the clients into clusters according to their influence scores. We adopt HDBSCAN because it does not require a pre-defined number of clusters, which is unknown in our setting. A key challenge for applying HDBSCAN is what distance metric should be used to measure the distance between two two-dimensional influence scores. To address this challenge, we propose a *scaled Euclidean distance*, which normalizes the two dimensions of a two-dimensional influence score to have the same, comparable scale. Subsequently, since malicious clients have large, positive influence scores s_i , we treat the clusters whose average s_i scores are positive as *potential malicious clusters*. However, the potential malicious clusters may also include Category I benign clients. To address the challenge, our key observation is that the influence-score gap $s'_i - s_i$ of a malicious client is smaller than that of a Category I benign client. FLForensics leverages this observation to further distinguish between malicious clients and Category I benign clients in the potential malicious clusters.

Theoretical and empirical evaluation. Theoretically, we show the security of FLForensics against poisoning attacks. In particular, based on a formal definition of poisoning attacks and mild assumptions, we show that 1) both malicious clients and Category I benign clients have larger influence scores s_i than Category II benign clients, and 2) a malicious client has a smaller influence-score gap $s'_i - s_i$ than a benign client. Empirically, we comprehensively evaluate FLForensics on five benchmark datasets. Our results show that FLForensics can accurately trace back malicious clients under various existing and adaptive attacks. We note that training-phase defenses are ineffective for most attack scenarios in our evaluation.

We summarize our main contributions as follows:

- We propose the first poison-forensics method called FLForensics to trace back malicious clients in FL.

- We theoretically show the security of FLForensics against poisoning attacks.
- We empirically evaluate FLForensics on five benchmark datasets against existing and adaptive poisoning attacks.

2 Preliminaries and Related Work

2.1 Federated Learning (FL)

In FL, training data is decentralized among n clients. The clients jointly learn a machine learning model (called *global model*) with the coordination of a server. In particular, the server maintains the global model while each client maintains a *local model* for its own local training data. In round t , the server sends its current global model w_t to the clients; a client i learns a local model $w_t^{(i)}$ by fine-tuning the global model to fit its local training data, i.e., $w_t^{(i)}$ has a small cross-entropy loss for its local training data, and sends the model update $g_t^{(i)} = w_t^{(i)} - w_t$ to the server; and the server aggregates the clients’ model updates to update the global model. Formally, the global model is updated as follows in training round t :

$$w_{t+1} = w_t + \alpha_t \cdot \text{Agg}(g_t^{(1)}, g_t^{(2)}, \dots, g_t^{(n)}), \quad (1)$$

where w_{t+1} is the global model after t training rounds, α_t is the learning rate in round t , Agg is an aggregation rule, and g_t^i is the model update from client i , where $i = 1, 2, \dots, n$. Note that the server may select a subset of clients in each round, in which the model updates of the selected clients are aggregated to update the global model. Different FL algorithms [1, 7–9] essentially use different aggregation rules Agg . For instance, FedAvg [1] uses the popular *average* aggregation rule, which uses the average of the clients’ model updates to update the global model. After training, the global model is deployed for real-world uses.

2.2 Poisoning Attacks to FL

Poisoning attacks to FL [4–6, 16] aim to compromise the training phase of an FL system such that a poisoned global model is learnt. In an *untargeted poisoning attack* [4], the poisoned global model misclassifies a large amount of testing inputs indiscriminately, leading to denial-of-service. In a *targeted poisoning attack* [5, 6, 16], the poisoned global model predicts an attacker-chosen label (called *target label*) for attacker-chosen *target inputs*, but its accuracy for non-target inputs is unaffected. In this work, we focus on targeted poisoning attacks due to their stealthiness and unless otherwise mentioned, we call them poisoning attacks for simplicity. Some poisoning attacks [5, 16] assume *any* input embedded with an attacker-chosen *trigger* as a target input, while some attacks [6] assume a small number of (e.g., 1) specific attacker-chosen inputs as target inputs. The former is also known as *backdoor attacks*.

Poisoning attacks with trigger-embedded target inputs: In these poisoning attacks, a target input is any input embedded with a trigger chosen by the attacker. For instance, in *scaling attack* [16], the attacker duplicates the training inputs on a malicious client, embeds a trigger into them, and sets their labels as the target label. Then, a malicious client trains a local model using the original training examples and the duplicated ones, and the malicious client scales the model update by a *scaling factor* λ before sending it to the server. The attacker in *a little is enough (ALIE) attack* [5] uses the same way to duplicate training examples and embed trigger into them on malicious clients, but the attacker solves an optimization problem to compute the model updates on malicious clients.

Poisoning attacks with triggerless target inputs: In these poisoning attacks, target inputs are specific inputs without an embedded trigger. For instance, the attacker in *edge attack* [6] augments the malicious clients’ local training data with a set of training examples (called *edge cases*) from a very different distribution. The attacker then changes the labels of the edge cases to the target label. A malicious client trains its local model using its local training data augmented with the edge cases labeled as the target label. The target inputs are inputs from this edge-case distribution.

2.3 Training-phase Defenses

Most existing defenses against poisoning attacks to FL aim to protect its training phase. The ultimate goal of these defenses is that a clean global model is learnt and deployed for practical uses. Specifically, one category of defenses [7–10, 17] aim to develop robust FL methods such that they are intrinsically robust against poisoning attacks. Another category of defenses [11, 18] aim to detect malicious clients during training and recover from attacks.

Robust FL: These defenses aim to *prevent* malicious clients from poisoning a global model during training. Specifically, some defenses—such as Trim [7], Median [7], FLTrust [9], and FLAME [8]—use Byzantine-robust aggregation rules instead of the average one to filter out potentially malicious model updates. These defenses can bound the difference between the global model learnt without malicious clients and the one learnt with malicious clients under some assumptions. Some provably robust defenses [10, 17] can guarantee a lower bound of testing accuracy no matter what poisoning attacks malicious clients use. For instance, Cao et al. [17] proposed to train multiple global models instead of a single one, each of which is trained using a subset of clients. Given a testing input, we take a majority vote among the multiple global models to predict its label.

Detecting malicious clients and recovering from attacks during training: For instance, FLDetector [11] aims to detect malicious clients that perform model poisoning attacks during training. The key intuition of FLDetector is that benign clients compute their model updates based on the pre-scribed FL algorithm and their local training data, but malicious clients in attacks craft their model updates without following the algorithm. Therefore, malicious clients’ model updates may not be consistent across multiple training rounds, which FLDetector exploits to detect malicious clients. After detecting malicious clients, FedRecover [18] can recover a clean global model efficiently without retraining from scratch.

Limitations: These training-phase defenses suffer from a few key limitations. As a result, the learnt global model may still be poisoned as shown in our experiments and the poisoned global model is deployed for practical uses. In particular, robust FL methods are still vulnerable to poisoning attacks when the number of malicious clients is large or the clients’ local training data is highly non-iid. Moreover, FLDetector fundamentally cannot detect data poisoning attacks, in which the malicious clients poison their local training data but follow the FL algorithm to compute the model updates.

Our work assumes a poisoned global model is deployed, and given a misclassified target input detected after model deployment, our work aims to trace back the malicious clients that performed the poisoning attack.

2.4 Poison Forensics for Centralized Learning

Poison forensics [19–21] has been studied for centralized learning. Specifically, given a misclassified target input detected after model deployment, some poison-forensics methods [19, 20] trace back the poisoned training examples. For instance, *Poison Forensics (PF)* [19] uses an iterative clustering and pruning method to identify the poisoned training examples that cause a given target input to be misclassified. GAS [20] uses renormalized influence estimator to pinpoint the labeled training examples that cause a misclassification. Given several trigger-embedded target inputs, some poison-forensics methods [21] aim to recover the trigger.

However, all these poison-forensics methods focus on centralized learning, where all training data is centralized at the server. When extended to FL, they achieve suboptimal performance as shown in our experiments. Our FLForensics is the first poison-forensics method to trace back malicious clients in FL. As a by-product of our work, we found that PF and GAS also achieve suboptimal performance for centralized learning when the training data is unbalanced. However, our FLForensics can still achieve good performance when extended to centralized learning in such scenarios (see Section 8 for more details).

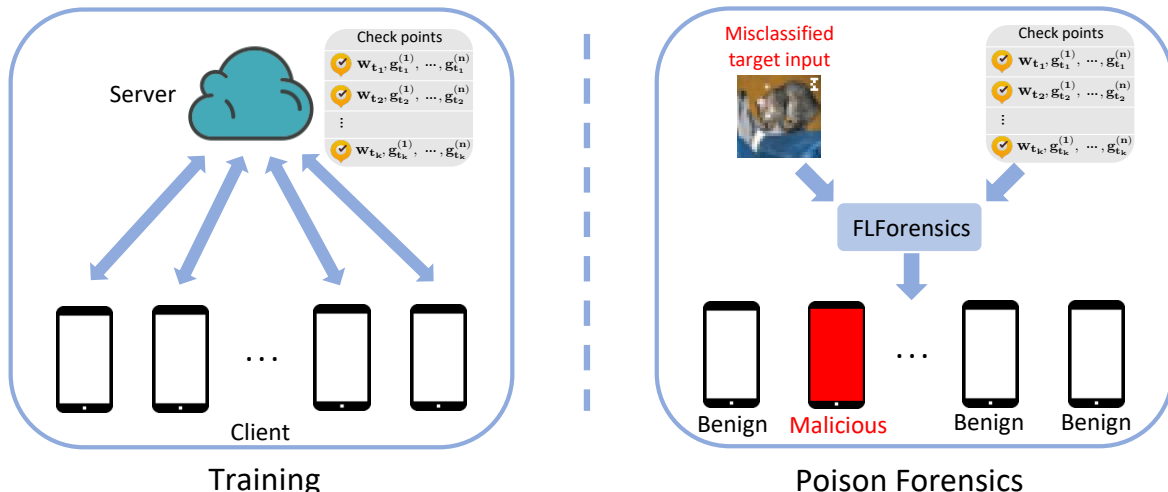


Figure 1: Overview of FLForensics. During training, the server stores the intermediate global models and clients’ model updates in some training rounds called *check points*. Given a misclassified target input detected after deploying the poisoned global model, the server uses FLForensics to trace back the malicious clients that performed the poisoning attack.

3 Threat Model

Poisoning attacks: We assume an attacker performs a poisoning attack during training. Specifically, the attacker controls some malicious clients, which could be compromised genuine clients or injected fake clients. The malicious clients send carefully crafted model updates to the server such that the global model is poisoned. We assume the server is not compromised. After training, the poisoned global model is deployed for real-world uses. In our work, we focus on targeted poisoning attacks, where the poisoned global model incorrectly classifies attacker-chosen target inputs as an attacker-chosen target label.

Poison forensics: We consider the following standard poison-forensics setting: a misclassified target input in a poisoning attack has been detected after model deployment. Such setting is commonly used in the poison forensics literature [19–21]. A misclassified target input can be detected by the server or a client via automatic detection methods [12–14] or manual analysis after model deployment. For instance, in Section 8, we show that our FLForensics can be adapted to detect whether a misclassified input is a misclassified target input or not. For manual analysis, a target input leads to misclassification and eventually error in the application that leverages the poisoned global model; and such error may be manually captured by a user/client. Given a misclassified target input, the server aims to trace back the malicious clients that performed the poisoning attack.

4 Our FLForensics

4.1 Overview

During training, FLForensics stores the intermediate global models and clients’ model updates in some training rounds, which we call *check points*. Given a misclassified target input, FLForensics traces back the malicious clients in two key steps: 1) calculating an *influence score* for each client and 2) detecting malicious clients based on the clients’ influence scores. In particular, a client’s influence score measures its “contribution” towards the given misclassification of the target input; and the server calculates an influence score for a client based on the global models and its model updates stored in the check points. Given the clients’ influence scores, we divide the clients into groups via a clustering method. The intuition is that benign clients and malicious ones form different clusters with respect to their influence

scores, e.g., malicious clients have large influence scores while benign ones have small influence scores. Based on the clustering results, we identify malicious clients. Figure 1 illustrates FLForensics, while Algorithm 1 summarizes its pseudo-code.

Algorithm 1 Our FLForensics

Input: Misclassified target input x , target label y , non-target input x' , check points $\Omega = \{t_1, t_2, \dots, t_k\}$, global models $\{w_t\}_{t \in \Omega}$ in the check points, selected clients C_t in each check point $t \in \Omega$, and clients' model updates $\{g_t^{(i)}\}_{t \in \Omega, i \in C_t}$.

Output: Predicted malicious clients \mathcal{M} .

- 1: //Calculating influence scores
- 2: **for** $i = 1$ to n **do**
- 3: $s_i = -\sum_{t \in \Omega \text{ s.t. } i \in C_t} \alpha_t \nabla \ell_{CE}(x, y; w_t)^\top g_t^{(i)}$;
- 4: $s'_i = -\sum_{t \in \Omega \text{ s.t. } i \in C_t} \alpha_t \nabla \ell_{CE}(x', y; w_t)^\top g_t^{(i)}$;
- 5: **end for**
- 6: $I \leftarrow \{(s_1, s'_1), (s_2, s'_2), \dots, (s_n, s'_n)\}$;
- 7: //Detecting malicious clients
- 8: $c_1, \dots, c_m, c_{outlier} \leftarrow \text{HDBSCAN}(I)$;
- 9: $c_{p_1}, c_{p_2}, \dots, c_{p_v} \leftarrow \text{clusters with average } s_i > 0$;
- 10: $threshold \leftarrow \sum_{j=1}^v \sum_{i \in c_{p_j}} s'_i / \sum_{j=1}^v \sum_{i \in c_{p_j}} s_i$;
- 11: $\mathcal{M} = \emptyset$;
- 12: **for** $j = 1$ to v **do**
- 13: $threshold_j \leftarrow \sum_{i \in c_{p_j}} s'_i / \sum_{i \in c_{p_j}} s_i$;
- 14: **if** $threshold_j \leq threshold$ **then** $\mathcal{M} = \mathcal{M} \cup c_{p_j}$;
- 15: **end if**
- 16: **end for**
- 17: **for** i in $c_{outlier}$ **do**
- 18: $threshold_i \leftarrow s'_i / s_i$;
- 19: **if** $threshold_i \leq threshold$ **then** $\mathcal{M} = \mathcal{M} \cup \{i\}$;
- 20: **end if**
- 21: **end for**
- 22: **return** \mathcal{M} ;

$\triangleright c_{outlier}$ is a set that contains all outliers if any.
 \triangleright Get potential malicious clusters.

4.2 Calculating Influence Scores

We denote a target input as x , which is misclassified as the target label y by the poisoned global model w .

Quantifying a misclassification using cross-entropy loss: A key challenge is how to quantify the misclassification so we can measure a client's contribution towards the misclassification as the client's influence score. To address the challenge, we quantify the misclassification using the loss of the global model. Specifically, we use the cross-entropy loss $\ell_{CE}(x, y; w)$ of the misclassified example (x, y) under the poisoned global model w . We adopt cross-entropy loss because it is widely used to train a model. The global model w is iteratively trained using the clients' model updates in multiple rounds. We denote by w_t the global model in training round t , where $t = 1, 2, \dots, R$. Suppose w_0 is the initialized global model and $\ell_{CE}(x, y; w_0)$ is the initialized loss for the target input x and target label y . After training R rounds, the loss changes to $\ell_{CE}(x, y; w_R)$. Our goal is to assign influence scores to the clients based on their contributions to the loss change $\ell_{CE}(x, y; w_0) - \ell_{CE}(x, y; w_R)$.

Expanding the training process: A client has a large influence score if it contributes more to the loss $\ell_{CE}(x, y; w_0) - \ell_{CE}(x, y; w_R)$. Since the loss change is accumulated over the R training rounds, we expand them to measure the

influence of each client on the loss change. Specifically, according to Taylor expansion, we have the following for each training round t :

$$\begin{aligned} \ell_{CE}(x, y; w_{t+1}) &\approx \ell_{CE}(x, y; w_t) \\ &\quad + \nabla \ell_{CE}(x, y; w_t)^\top (w_{t+1} - w_t), \end{aligned} \quad (2)$$

where $\nabla \ell_{CE}(x, y; w_t)^\top$ is the transpose of $\nabla \ell_{CE}(x, y; w_t)$ and w_t is the global model in training round t . Therefore, by summing over R training rounds on both sides of the above equation, we have the loss change as follows:

$$\begin{aligned} \ell_{CE}(x, y; w_0) - \ell_{CE}(x, y; w_R) \\ \approx - \sum_{t=1}^R \nabla \ell_{CE}(x, y; w_t)^\top (w_{t+1} - w_t), \end{aligned} \quad (3)$$

where R is the total number of training rounds.

Assigning influence scores: Different clients contribute differently to the model difference $w_{t+1} - w_t$ in the t th training round. Therefore, different clients contribute differently to the loss change. Our method quantifies the contribution of a client to the model difference $w_{t+1} - w_t$ in a training round and obtain an influence score for a client by summing over such contributions over multiple training rounds that involve the client. We say a client is involved in a training round if it is selected in this training round.

Suppose the server selects a subset (denoted as C_t) of clients in training round t . Recall that the global model is updated using Equation 1, where *Agg* uses the selected clients C_t . Therefore, to measure the contribution of client i on the model difference $w_{t+1} - w_t$, we assume the global model is updated as if using only the model update $g_t^{(i)}$ of client i , i.e., $w_{t+1} - w_t \approx \alpha_t \cdot g_t^{(i)}$. Thus, based on Equation 3, we have the influence score s_i for client i as follows:

$$s_i = - \sum_{t \text{ s.t. } i \in C_t} \alpha_t \nabla \ell_{CE}(x, y; w_t)^\top g_t^{(i)}. \quad (4)$$

Using check points to save space and computation: Note that using all training rounds to calculate the influence scores suffers from a space and computation efficiency issue. Specifically, the server needs to save the global models and clients' model updates in all training rounds during training, which incurs substantial space and computation overhead. To mitigate this issue, the server can save the global models and clients' model updates in a subset of training rounds, which we call *check points*. Then, we can use the check points to calculate the influence scores. Formally, we have:

$$s_i = - \sum_{t \in \Omega \text{ s.t. } i \in C_t} \alpha_t \nabla \ell_{CE}(x, y; w_t)^\top g_t^{(i)}, \quad (5)$$

where $\Omega = \{t_1, t_2, \dots, t_k\}$ is the set of k check points. FLForensics incurs space overhead for the server due to storing global models and clients' model updates in the check points. The space overhead is linear to the model size, number of check points, and the number of clients selected to participate in each training round. This storage overhead is acceptable for a powerful server. In Section 8, we discuss the potential privacy concerns of storing check points.

Using a non-target input to augment clients' influence scores: A unique characteristics of FL is that the clients' local training data may have different distributions, i.e., non-iid. In particular, some benign clients (denoted as *Category I*) may have a large fraction of local training examples with the attacker-chosen target label, while other benign clients (denoted as *Category II*) do not. While Category II benign clients do not contribute to the misclassification loss of the target input, Category I benign clients may contribute substantially to the misclassification loss since their model updates are likely to make any input predicted as the target label. As a result, both Category I benign clients and malicious clients have large influence scores as defined in Equation 5. In particular, our theoretical analysis in

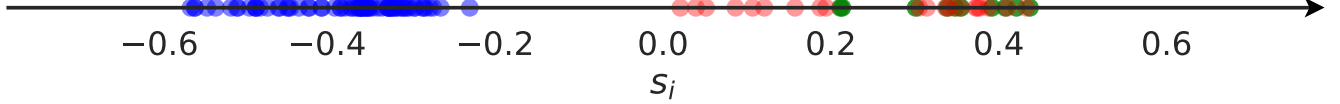


Figure 2: Influence scores s_i of malicious clients (red dots), Category I benign clients (green dots), and Category II benign clients (blue dots) in one of our experiments.

Section 5 shows that they both have larger influence scores than Category II benign clients. As a result, Category I benign clients and malicious clients are indistinguishable with respect to the influence scores s_i , which is also confirmed by our experimental results. For instance, Figure 2 shows such influence scores s_i of malicious clients, Category I benign clients, and Category II benign clients in one of our experiments.

To address the challenge, we propose that the server further uses another *non-target input* to calculate influence scores. Our intuition is that, for such a non-target input, Category I benign clients still have large influence scores, but the malicious clients have small influence scores since the input is a non-target one. Therefore, we can distinguish between Category I benign clients and malicious clients. The non-target input can be a random input or a true input with the target label from the learning task’s data distribution. We show in Section 8, FLForensics achieves comparable results in most cases when using a random input or a true input as the non-target input. We denote the non-target input as x' . Moreover, we denote by s'_i the influence score for client i calculated based on the non-target input x' . According to Equation 5, we have:

$$s'_i = - \sum_{t \in \Omega \text{ s.t. } i \in C_t} \alpha_t \nabla \ell_{CE}(x', y; w_t)^\top g_t^{(i)}, \quad (6)$$

where $\Omega = \{t_1, t_2, \dots, t_k\}$ is the set of k check points. To summarize, the influence score for a client i is a two-dimensional vector (s_i, s'_i) .

4.3 Detecting Malicious Clients

Intuitively, a malicious client i has a large influence score s_i but a small s'_i ; a Category I benign client i has large both s_i and s'_i ; and a Category II benign client i has small both s_i and s'_i . In other words, we have two key observations as follows:

- **Observation I.** Both malicious clients and Category I benign clients have larger influence scores s_i than Category II benign clients.
- **Observation II.** Malicious clients have smaller influence score gaps $s'_i - s_i$ than benign clients.

We theoretically show the two observations hold based on a formal definition of poisoning attacks and mild assumptions in Section 5. Based on such observations, we propose a clustering-based method to detect malicious clients.

Clustering the clients via HDBSCAN with scaled Euclidean distance: We denote the influence scores of the n clients as $I = \{(s_1, s'_1), (s_2, s'_2), \dots, (s_n, s'_n)\}$. We first divide the clients into clusters based on their two-dimensional influence scores. In particular, we use HDBSCAN [15] as the clustering method. We select HDBSCAN because it

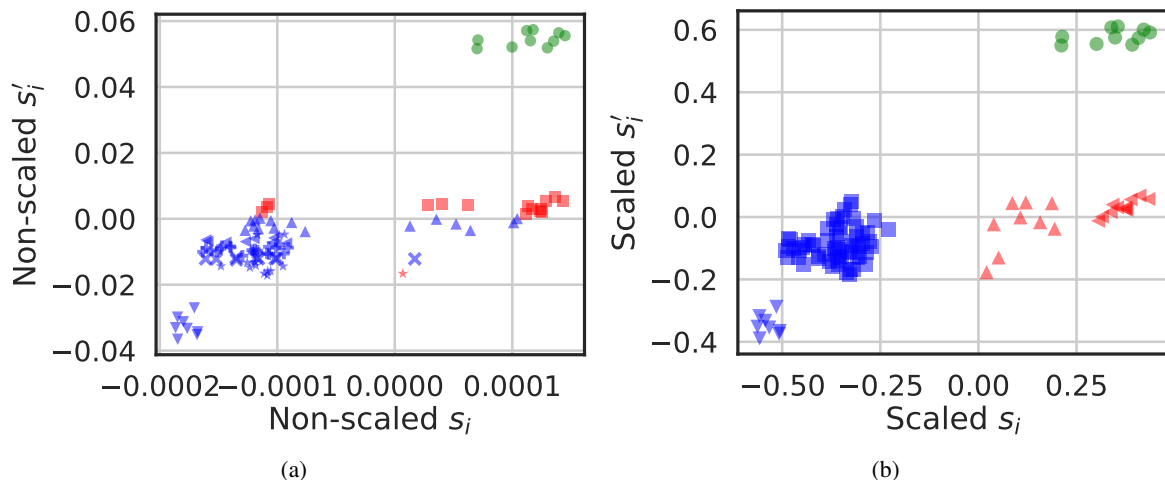


Figure 3: Clustering results in one of our experiments when (a) Euclidean distance is used and (b) scaled Euclidean distance is used. Each dot represents a client. Red dots are malicious clients, green dots are Category I benign clients, and blue dots are Category II benign clients. Different markers represent different clusters obtained from HDBSCAN.

does not require specifying the number of clusters, which we may not know in advance. HDBSCAN allows us to specify a metric to measure the distance between two two-dimensional influence scores. To consider the different scales of the two dimensions, we use *scaled Euclidean distance* as the distance metric. Specifically, we scale each influence score s_i by the span of the influence scores, i.e., s_i is scaled as $s_i / (\max_{j=1}^n s_j - \min_{j=1}^n s_j)$; and similarly, we scale s'_i as $s'_i / (\max_{j=1}^n s'_j - \min_{j=1}^n s'_j)$. Then, we compute the Euclidean distance between two two-dimensional scaled influence scores in HDBSCAN. Figure 3 illustrates the clustering results in one of our experiments when using the standard Euclidean distance and our scaled Euclidean distance. In this example, the malicious clients are grouped in clusters using scaled Euclidean distance while they are mixed with benign clients when Euclidean distance is used.

Identifying malicious clients and Category I benign clients based on Observation I: Since malicious clients have large, positive influence scores s_i , we treat the clusters whose average s_i scores are positive as *potential malicious clusters*. The clients in these clusters are potential malicious because Category I benign clients may also have large, positive influence scores. In other words, a potential malicious cluster may include malicious clients or Category I benign clients. For instance, in our example in Figure 3b, both the red clusters (malicious clients) and the green cluster (Category I benign clients) are potential malicious clusters.

Distinguishing between malicious clients and Category I benign clients based on Observation II: Finally, we further distinguish between malicious clients and Category I benign clients in the potential malicious clusters. Our key observation is that the influence-score difference between s'_i and s_i of malicious clients is smaller than that of Category I benign clients. Based on this observation, for each potential malicious cluster, we compute the ratio between the average s'_i and the average s_i of the clients in the cluster. Intuitively, such ratio of a malicious cluster is smaller than that of a Category I benign cluster. In particular, when the ratio is no larger than a *threshold*, we identify the clients in the corresponding cluster as malicious. The key challenge is how to determine the threshold. If the threshold is too large, then some benign clusters may be falsely identified as malicious; and if the threshold is too small, then some malicious clusters may be falsely identified as benign. To address the challenge, we use all potential malicious clusters to determine the threshold. In particular, we treat the ratio between the average s'_i and the average s_i of the clients in all potential malicious clusters as the threshold. Our way of determining the threshold essentially treats a potential malicious cluster, whose s'_i/s_i ratio is below the s'_i/s_i ratio among all potential malicious clusters, as malicious. In our example in Figure 3b, our method correctly identifies the red clusters as malicious.

Note that HDBSCAN may classify some clients as outliers, which do not belong to any cluster. For each outlier,

we calculate its influence score ratio s'_i/s_i . If this ratio is equal to or less than the previously determined threshold, we identify the outlier as malicious.

5 Theoretical Analysis

FLForensics leverages the Observation I and II. We theoretically show that they hold under a formal definition of poisoning attack and some mild assumptions, which theoretically explains the effectiveness of FLForensics. We acknowledge that these assumptions may not hold in practice, and thus we empirically show the effectiveness of FLForensics in such scenarios in our experiments in Section 6.2. Next, we first introduce a formal definition of poisoning attack to FL and two assumptions. Then, we describe our theorems.

5.1 Formal Definition and Assumptions

Definition 1 (Poisoning Attack to FL). *In a poisoning attack, malicious clients aim to poison the global model w such that it predicts target label y for any target input x , i.e., the loss $\ell_{CE}(x, y; w)$ is small; and benign clients aim to learn the global model such that it is accurate for non-target true inputs, i.e., the loss $\ell_{CE}(x', y; w)$ is small. Therefore, in a training round, a malicious client's model update does not increase the loss $\ell_{CE}(x, y; w)$ for a target input, while a benign client's model update does not decrease such loss. On the contrary, a malicious client's model update does not decrease the loss $\ell_{CE}(x', y; w)$, while a benign client's model update does not increase such loss. Formally, for any check-point training round $t \in \Omega$, malicious client i , and benign client j , we have the following assumptions to characterize the training process:*

$$\ell_{CE}(x', y; w_t + g_t^{(j)}) \leq \ell_{CE}(x', y; w_t + g_t^{(i)}), \quad (7)$$

$$\ell_{CE}(x, y; w_t + g_t^{(j)}) \geq \ell_{CE}(x, y; w_t + g_t^{(i)}), \quad (8)$$

where $w_t + g_t^{(i)}$ and $w_t + g_t^{(j)}$ respectively are the global models after training round t if only the model updates of clients i and j were used to update the global model.

Assumption 1 (Local Linearity). *We assume the cross-entropy losses $\ell_{CE}(x', y; w_t)$ and $\ell_{CE}(x, y; w_t)$ are locally linear in the region around w_t . In particular, based on first-order Taylor expansion, we have the following:*

$$\ell_{CE}(x', y; w_t + \delta) = \ell_{CE}(x', y; w_t) + \nabla \ell_{CE}(x', y; w_t)^\top \delta,$$

$$\ell_{CE}(x, y; w_t + \delta) = \ell_{CE}(x, y; w_t) + \nabla \ell_{CE}(x, y; w_t)^\top \delta.$$

We note that the local linearity assumption was also used in the machine learning community [22, 23].

Assumption 2 (Label-rich Advantage). *According to the definitions of Category I and Category II benign clients, a Category I benign client possesses a larger fraction of local training examples with the target label y compared to a Category II benign client. Therefore, given any target input x with target label y , we assume that the local model of a Category I benign client is more likely to predict x as y than that of a Category II benign client. Formally, for any check-point training round $t \in \Omega$, Category I benign client j_1 , and Category II benign client j_2 , we make the following assumption:*

$$\ell_{CE}(x, y; w_t + g_t^{(j_1)}) \leq \ell_{CE}(x, y; w_t + g_t^{(j_2)}), \quad (9)$$

where $w_t + g_t^{(j_1)}$ is the local model of Category I benign client j_1 and $w_t + g_t^{(j_2)}$ is the local model of Category II benign client j_2 in the training round t .

5.2 Theoretical Analysis on Observation I

Theorem 1 and 2 together show that Observation I holds.

Theorem 1. *Suppose the server picks all clients in each check-point training round, i.e., $C_t = \{1, 2, \dots, n\}$ for $t \in \Omega$, and FLForensics uses a true non-target input with target label y . Based on the poisoning attack definition and Assumption 1, we have that the influence score s_i of a malicious client i is no smaller than the influence score s_j of a Category II benign client j . Concretely, we have:*

$$s_i \geq s_j, \quad (10)$$

where s_i and s_j are computed based on Equation 5.

Proof. Please see Appendix A.1. □

Theorem 2. *Suppose the server picks all clients in each check-point training round, i.e., $C_t = \{1, 2, \dots, n\}$ for $t \in \Omega$, and FLForensics uses a true non-target input with target label y . Based on Assumption 1 and Assumption 2, we have that the influence score s_{j_1} of a Category I benign client j_1 is no smaller than the influence score s_{j_2} of a Category II benign client j_2 . Specifically, we have:*

$$s_{j_1} \geq s_{j_2}, \quad (11)$$

where s_{j_1} and s_{j_2} are computed based on Equation 5.

Proof. Please see Appendix A.2. □

5.3 Theoretical Analysis on Observation II

Theorem 3. *Suppose the server picks all clients in each check-point training round, i.e., $C_t = \{1, 2, \dots, n\}$ for $t \in \Omega$, and FLForensics uses a true non-target input with target label y . Based on the poisoning attack definition and Assumption 1, we have the influence score gap $s'_i - s_i$ of a malicious client i is no larger than the influence score gap $s'_j - s_j$ of a benign client j . Formally, we have:*

$$s'_i - s_i \leq s'_j - s_j, \quad (12)$$

where s_i and s_j are computed based on Equation 5, while s'_i and s'_j are computed based on Equation 6.

Proof. Please see Appendix A.3. □

Corollary 1. *Given a malicious client i and a benign client j , if the influence scores $s_i > 0$ and $s_j > 0$, then the influence score ratios satisfy: $\frac{s'_i}{s_i} \leq \frac{s'_j}{s_j}$.*

Proof. Please see Appendix A.4. □

Remark. *Corollary 1 explains why FLForensics can distinguish between malicious clients and Category I benign clients. Specifically, malicious clients and Category I benign clients are in potential malicious clusters, which may have positive influence scores (see Figure 3b and Line 9 of Algorithm 1). Therefore, the influence score ratios can be used to distinguish between them based on Corollary 1.*

Table 1: Dataset statistics.

Dataset	# Training	# Testing	# Classes
CIFAR-10	50,000	10,000	10
Fashion-MNIST	60,000	10,000	10
MNIST	60,000	10,000	10
Sentiment140	72,491	358	2
ImageNet-Fruits	13,000	500	10

6 Experiments

6.1 Experimental Setup

Datasets: We use five benchmark datasets in our experiments, comprising four image datasets and one text dataset. Table 1 provides an overview of the dataset statistics.

CIFAR-10 [24]. This is a commonly employed dataset in image classification task, comprising 50,000 training examples and 10,000 testing examples. Each input is a 3-channel color image of 32×32 pixels in size and belongs to one of ten classes.

Fashion-MNIST [25]. This dataset consists of 70,000 grayscale images of fashion items, with 60,000 for training and 10,000 for testing. Each input is of 28×28 pixels in size and belongs to one of ten classes.

MNIST [26]. Like Fashion-MNIST, MNIST also contains 70,000 1-channel grayscale images, split into 60,000 training examples and 10,000 testing examples. Each input is a 28×28 pixel image of a handwritten digit. The dataset includes ten classes with each class corresponding to a digit from 0 to 9.

Sentiment140 [27]. This is a two-class text classification dataset for sentiment analysis. This dataset is collected from Twitter users. In our experiments, we adopt users with at least 50 tweets, which results in 927 users. Each user has a pre-defined set of the training and testing tweets. For our considered users, we have 72,491 training tweets and 358 testing tweets in total.

ImageNet-Fruits [28]. This is an image classification dataset comprising 128×128 pixel color images. It represents a subset of the larger ImageNet-1k [29] dataset, specifically curated to include ten fruit categories, such as ‘pineapple’, ‘banana’, and ‘cucumber’.

FL training settings: Following prior work [4, 9], we assume 100 clients in total. A unique characteristic of FL is that the local training data are not identically distributed (non-iid) across clients. We use the method in [4] to simulate non-iid settings, and the degree of non-iid is set to 0.5 for CIFAR-10, Fashion-MNIST, MNIST, and ImageNet-Fruits. The details of simulating non-iid can be found in Appendix A.6. For the Sentiment140 dataset, we divide the users into 100 groups uniformly at random. Each group is considered as a client, whose local training data is the union of the training tweets of the users in the group. Users’ tweets are non-iid, so the clients’ local training data are also non-iid. Therefore, we do not need to simulate the non-iid setting for this dataset. We train a ResNet-20 [30] classifier for CIFAR-10, a CNN classifier for Fashion-MNIST and MNIST (the architecture is shown in Table 15 in Appendix), a LSTM [31] classifier for Sentiment140, and a ResNet-50 [30] classifier for ImageNet-Fruits dataset.

The default parameter settings (e.g., learning rates, batch sizes, global rounds, and local training epochs) are shown in Table 16 in Appendix. By default, the server selects all clients in each training round and uses the average aggregation rule FedAvg [1] to aggregate the clients’ model updates. However, we will explore the impact of the fraction of selected clients in a training round and aggregation rule on FLForensics.

Poisoning attacks to FL: We consider three popular poisoning attacks to FL, i.e., *Scaling* [16], *A little is enough (ALIE)* [5], and *Edge* [6] attacks. Scaling and ALIE use trigger-embedded target inputs, while Edge uses triggerless target inputs.

Scaling [16]. Following [16], the attacker duplicates local training inputs on the malicious clients, embeds the trigger into them, and sets their labels as the target label. Then, a malicious client trains its local model using the original local training examples and the duplicated ones following FL algorithm; and a malicious client scales its model update by a factor γ before sending it to the server. By default, we set $\gamma = 1$ since this setting makes it hard to detect the malicious clients during training but the attack is still successful. We will also explore its impact on FLForensics. Specifically, we follow [16] and [32] to set and embed the triggers for CIFAR-10 and Fashion-MNIST, respectively. For MNIST and ImageNet-Fruits, the triggers are shown in Figure 4a and Figure 4b in Appendix, respectively. For Sentiment140, we use “debug FLpoisoning” as a trigger and replace two random consecutive words as the trigger in each duplicated training input. The target labels of CIFAR-10, Fashion-MNIST, MNIST, Sentiment140, and ImageNet-Fruits are set to 2, 0, 0, “negative”, and 2, respectively.

A little is enough (ALIE) [5]. The attacker in ALIE attack uses the same strategy as that in Scaling attack to embed the triggers into duplicated local training inputs and set their labels as target labels on the malicious clients. However, instead of scaling the model updates, the malicious clients carefully craft their model updates via solving an optimization problem.

Edge [6]. The attacker in Edge attack injects some training examples (called *edge-case examples*) labeled as the target label into the malicious clients’ local training data, which are from a distribution different from that of the learning task’s overall training data. Each malicious client trains its local model using the original local training examples and the edge-case ones following the FL algorithm. In our experiments, for CIFAR-10 and Sentiment140 datasets, we use the edge-case examples respectively designed for CIFAR-10 and Sentiment140 datasets in [6]. For the Fashion-MNIST and MNIST datasets, we use the edge-case examples designed for EMNIST dataset in [6]. For ImageNet-Fruits dataset, we use unripe banana images from [33] as edge-case examples and label them as ‘cucumber’. The target inputs are from the same dataset as the edge-case examples.

By default, we assume there are 20% malicious clients, who perform attacks in each training round. We will also explore the impact of the fraction of malicious clients and fraction of attacked training rounds on FLForensics.

Compared methods: We compare FLForensics with the following methods including variants of FLForensics.

Poison Forensics (PF) [19]. PF is a poison-forensics method for centralized learning. We extend PF to FL by assuming the server has access to clients’ local training data. Given a global model, the clients’ local training data, and a misclassified target input, we use PF to detect the poisoned training examples. Then, we classify a client as malicious if its fraction of detected poisoned local training examples is larger than the overall fraction of detected poisoned training examples among all clients.

FLForensics-G (GAS [20] + FLForensics). GAS is a method to compute influence scores for labeled training examples in centralized learning. We extend GAS to FL by assuming the server has access to the clients’ local training data. However, GAS does not detect poisoned training examples based on the influence scores (i.e., no second step in FLForensics). Therefore, we combine GAS and FLForensics as an end-to-end method. Given a global model, the clients’ local training data, and a misclassified target input, we use GAS to compute an influence score for each labeled training example. Then, we detect the poisoned training examples using HDBSCAN based on the influence scores of these examples (Appendix A.5 shows more details). A client is classified as malicious if its fraction of the detected poisoned local training examples is larger than the overall fraction of the detected poisoned training examples.

FLForensics-A. This is a variant of FLForensics, which only uses a target input x to detect malicious clients. Specifically, the server computes the influence score s_i for each client i based on Equation 5, uses HDBSCAN to divide the clients into clusters based on the influence scores, and treats the clusters whose average influence scores are positive as malicious. We evaluate this variant to show that a target input alone is insufficient.

Evaluation metrics: Our method and compared ones classify clients into malicious and benign. Therefore, we adopt *detection accuracy (DACC)*, *false positive rate (FPR)*, and *false negative rate (FNR)* as our evaluation metrics. DACC is the fraction of clients that are correctly classified, FPR is the fraction of benign clients that are classified as malicious, and FNR is fraction of malicious clients that are classified as benign. A larger DACC and smaller FPR/FNR indicate a better method. We also use *attack success rate (ASR)* to measure success of a poisoning attack, where ASR

is the fraction of target inputs that are predicted as the target label.

Poison-forensics settings: In our experiments, we randomly pick a misclassified target input for each dataset. Our method also requires a non-target input. We generate an input uniformly at random as the non-target input since the server may not have access to a true input from the learning task’s distribution. Specifically, for the image datasets, we generate a random input by sampling each pixel value from a uniform distribution; and for the text dataset, we generate a random input as a random tweet that has the same length as the given misclassified target input. We will also explore using a true input as a non-target input in Section 8, and our results show that FLForensics further improves slightly in some scenarios. FLForensics saves check points during training. By default, the server saves the global model and clients’ model updates every 10 training rounds. To reduce the impact of the magnitude variances of the model updates $g_t^{(i)}$ across clients i and training rounds t , we normalize $g_t^{(i)}$ to have ℓ_2 norm of 1 in Equation 5 and 6. Unless otherwise mentioned, we report the results on CIFAR-10 dataset under Scaling attack.

6.2 Experimental Results

Training-phase defenses are insufficient: Training-phase defenses use robust FL methods or malicious-client detection methods to prevent malicious clients from poisoning a global model during training. Table 18 in Appendix shows that robust FL methods—such as Trim [7], Median [7], FLTrust [9], and FLAME [8]—are insufficient. In particular, ASRs of the considered poisoning attacks are still high in many cases. Table 2 shows that FLDetector, a malicious-client detection method, cannot accurately detect malicious clients during training in many cases. These training-phase defenses are still vulnerable to poisoning attacks because the clients’ training data are non-iid, making it hard to accurately distinguish between malicious clients’ and benign clients’ model updates.

Table 2: Results of FLDetector, a training-phase method to detect malicious clients. Table 18 in Appendix shows the results for robust FL methods. Our results show that training-phase defenses are insufficient at defending against poisoning attacks.

Dataset	Scaling attack			ALIE attack			Edge attack		
	DACC	FPR	FNR	DACC	FPR	FNR	DACC	FPR	FNR
CIFAR-10	0.400	0.538	0.850	0.000	1.000	1.000	0.160	0.800	1.000
Fashion-MNIST	0.870	0.138	0.100	0.000	1.000	1.000	0.390	0.563	0.800
MNIST	0.960	0.038	0.050	0.000	1.000	1.000	0.160	0.800	1.000
Sentiment140	0.020	0.975	1.000	0.010	0.988	1.000	0.080	0.900	1.000
ImageNet-Fruits	0.475	0.438	0.875	0.075	0.906	1.000	0.750	0.281	0.250

FLForensics is effective: Table 3 shows the results of FLForensics and compared poison-forensics methods under different attacks and datasets. We observe that FLForensics can accurately identify malicious clients, achieving a DACC of 1 or nearly 1 in all experiments. The FPR of FLForensics is 0 or close to 0 in most cases, with four exceptions (Sentiment140 dataset under Scaling attack, Sentiment140 dataset under Edge attack, CIFAR-10 dataset under Edge attack, and ImageNet-Fruits dataset under Edge attack), for which FPR is around 3%, i.e., one to three benign clients are misclassified as malicious. Similarly, FNR is also 0 or close to 0, with only two exceptions.

FLForensics outperforms the compared poison-forensics methods: Table 3 also shows that our FLForensics outperforms the compared poison-forensics methods. First, FLForensics outperforms FLForensics-A, particularly evident in FLForensics’s significantly lower FPR compared to FLForensics-A. For instance, FLForensics exhibits a FPR of 0 under all attacks on CIFAR-10, while FLForensics-A’s FPR consistently exceeds 10%, indicating that at least 8 benign clients are incorrectly classified as malicious clients by FLForensics-A. This result demonstrates that using only the target input x is unable to distinguish between malicious and Category I benign clients. Second, FLForensics outperforms PF and FLForensics-G because they were not designed for FL. In our comparison, we give advantages to FLForensics-G and PF by assuming that they have access to the local training data. We also conduct

Table 3: Results of FLForensics and compared poison-forensics methods.

Dataset	Method	Scaling attack			ALIE attack			Edge attack		
		DACC	FPR	FNR	DACC	FPR	FNR	DACC	FPR	FNR
CIFAR-10	PF	0.900	0.125	0.000	0.900	0.125	0.000	0.820	0.225	0.000
	FLForensics-G	0.900	0.125	0.000	0.900	0.125	0.000	0.920	0.100	0.000
	FLForensics-A	0.900	0.125	0.000	0.900	0.125	0.000	0.910	0.113	0.000
	FLForensics	1.000	0.000	0.000	1.000	0.000	0.000	0.980	0.000	0.100
Fashion-MNIST	PF	0.900	0.125	0.000	0.900	0.125	0.000	1.000	0.000	0.000
	FLForensics-G	0.740	0.100	0.900	0.740	0.100	0.900	0.920	0.100	0.000
	FLForensics-A	1.000	0.000	0.000	1.000	0.000	0.000	0.920	0.100	0.000
	FLForensics	1.000	0.000	0.000	1.000	0.000	0.000	1.000	0.000	0.000
MNIST	PF	0.900	0.125	0.000	0.740	0.325	0.000	0.920	0.100	0.000
	FLForensics-G	0.480	0.413	0.950	0.520	0.363	0.950	0.930	0.088	0.000
	FLForensics-A	0.900	0.125	0.000	0.900	0.125	0.000	0.920	0.100	0.000
	FLForensics	1.000	0.000	0.000	1.000	0.000	0.000	1.000	0.000	0.000
Sentiment140	PF	0.990	0.013	0.000	0.760	0.275	0.100	0.970	0.038	0.000
	FLForensics-G	0.990	0.013	0.000	0.980	0.025	0.000	0.940	0.075	0.000
	FLForensics-A	0.900	0.125	0.000	0.900	0.125	0.000	0.920	0.100	0.000
	FLForensics	0.980	0.025	0.000	1.000	0.000	0.000	0.970	0.038	0.000
ImageNet-Fruits	PF	0.600	0.375	0.500	1.000	0.000	0.000	0.850	0.188	0.000
	FLForensics-G	0.600	0.313	0.750	0.525	0.406	0.750	0.700	0.125	1.000
	FLForensics-A	0.900	0.125	0.000	0.875	0.156	0.000	0.800	0.125	0.500
	FLForensics	1.000	0.000	0.000	1.000	0.000	0.000	0.950	0.031	0.125

Table 4: Impact of the number of check points.

# check points	DACC	FPR	FNR
10	0.970	0.038	0.000
50	1.000	0.000	0.000
150	1.000	0.000	0.000

Table 5: Storage overhead of FLForensics.

Dataset	# check points	# clients	Storage overhead (GB)
CIFAR-10	150	100	15.22
Fashion-MNIST	200	100	10.43
MNIST	200	100	10.43
Sentiment140	150	100	3.02
ImageNet-Fruits	100	40	22.20

experiments where they use clients’ model updates sent to the server. Table 17 in Appendix shows the results. We can observe that FLForensics-G performs worse, while PF achieves similar performance to using the local training data.

Impact of number of check points and storage overhead: Table 4 shows the impact of the number of check points on FLForensics. We observe a trade-off between storage overhead and poison-forensics performance. In particular, when a server saves more check points, which incurs more storage overhead, the server can more accurately detect the malicious clients. We also note that the storage overhead is acceptable for a powerful server to achieve good poison-forensics performance. Table 5 shows the storage overhead for different datasets in our default settings. For instance, saving 150 check points for CIFAR-10 requires 15.22GB storage, which is acceptable for a powerful server like a data center.

Impact of fraction of malicious clients: Table 6 shows the impact of fraction of malicious clients on FLForensics. We observe that FLForensics works well when a large fraction of clients are malicious. For instance, only 5% of malicious

Table 6: Impact of the fraction of malicious clients.

Fraction of malicious clients	DACC	FPR	FNR
10%	1.000	0.000	0.000
20%	1.000	0.000	0.000
30%	0.990	0.000	0.033
40%	0.980	0.000	0.050

Table 7: Impact of degree of non-iid.

Degree of non-iid	DACC	FPR	FNR
0.1	1.000	0.000	0.000
0.3	1.000	0.000	0.000
0.5	1.000	0.000	0.000
0.7	0.970	0.000	0.150

Table 8: Impact of different aggregation rules.

Aggregation rule	DACC	FPR	FNR
Trim	1.000	0.000	0.000
Median	1.000	0.000	0.000
FLTrust	1.000	0.000	0.000
FLAME	0.970	0.038	0.000

Table 9: Impact of fraction of selected clients.

Fraction of clients	DACC	FPR	FNR
10%	1.000	0.000	0.000
20%	1.000	0.000	0.000
40%	1.000	0.000	0.000
60%	1.000	0.000	0.000
100%	1.000	0.000	0.000

Table 10: Impact of scaling factor γ in Scaling attack.

γ	DACC	FPR	FNR
0.5	1.000	0.000	0.000
1.0	1.000	0.000	0.000
5.0	1.000	0.000	0.000
15.0	1.000	0.000	0.000
40.0	1.000	0.000	0.000

clients are identified as benign even if 40% of clients are malicious. Moreover, all benign clients are correctly detected as benign (i.e., FPR=0) when the fraction of malicious clients varies from 10% to 40%. We note that when the fraction of malicious clients is small, the attacks are not effective [4], and thus we consider at least 10% of malicious clients.

Impact of degree of non-iid: Based on the results in Table 7, FLForensics works well across different degrees of non-iid. In particular, FLForensics achieves 0 FPR and at most 15% FNR across different settings of degree of non-iid. Note that 0.1 degree of non-iid represents the iid setting. FLForensics works well for non-iid because it is explicitly designed to take non-iid into consideration.

Impact of aggregation rules: Based on Table 8, FLForensics can accurately trace back the malicious clients when the server uses different Byzantine-robust aggregation rules during training. We note that these Byzantine-robust aggregation rules are not effective at defending against the poisoning attacks in our experimental settings, as shown in Table 18 in Appendix. Our results show that FLForensics is complementary with training-phase defenses and can be used together with them. In Table 8, FLForensics achieves slightly higher FPR when FLAME is used as the aggregation rule. This is because Scaling attack is less effective for FLAME and FLForensics incorrectly identifies some Category I benign clients as malicious.

Impact of fraction of selected clients: Based on Table 9, FLForensics works well even if the server selects a small fraction of clients in each training round. The reason is that once a malicious client appears in multiple check-point training rounds, FLForensics can accumulate its influences to distinguish it with benign clients. Note that in this experiment, we save all training rounds as check points so a malicious client appears in multiple of them.

Impact of scaling factor γ : Based on the results in Table 10, we observe that FLForensics works well for a wide range of scaling factors used by the Scaling attack. The reason is that once the Scaling attack is effective, FLForensics can identify the malicious clients. Previous work [16] shows that the higher the scaling factor, the more effective the attack, but it also makes the attack more susceptible to detection. We can observe that our FLForensics can detect all the malicious clients even when the scaling factor is close to 1. In such cases, methods (e.g., FLDetector) that rely on the magnitudes of clients' model updates to detect malicious clients often fail.

Recovering from attacks after FLForensics: After detecting malicious clients, a server can re-train a global model using the remaining clients to recover from attacks. We pick the case in Table 3, for which FLForensics has

Table 11: Results of FLForensics for adaptive attacks.

(a) Different attack frequencies

Attack frequency	DACC	FPR	FNR	ASR
Attack in every round	1.000	0.000	0.000	0.682
Attack in every 2 rounds	1.000	0.000	0.000	0.731
Attack in every 5 rounds	1.000	0.000	0.000	0.730
Attack in every 10 rounds	0.900	0.125	0.000	0.116

(b) Different attack probabilities

Attack probability	DACC	FPR	FNR	ASR
1.0	1.000	0.000	0.000	0.682
0.8	0.990	0.000	0.050	0.612
0.5	0.970	0.013	0.100	0.545
0.2	0.920	0.013	0.350	0.200





(c) Different trigger locations

Trigger location	DACC	FPR	FNR	ASR
UR	1.000	0.000	0.000	0.682
LR	1.000	0.000	0.000	0.884
UL	1.000	0.000	0.000	0.161
LL	1.000	0.000	0.000	0.861
Random	0.940	0.000	0.300	0.102

(d) Different trigger sizes

Trigger size	DACC	FPR	FNR	ASR
2×2	0.700	0.125	1.000	0.001
3×3	1.000	0.000	0.000	0.142
5×5	1.000	0.000	0.000	0.278
10×10	1.000	0.000	0.000	0.685

(e) Different trigger values

Trigger value	DACC	FPR	FNR	ASR
	1.000	0.000	0.000	0.682
	1.000	0.000	0.000	0.308
	0.700	0.125	1.000	0.000
	1.000	0.000	0.000	1.000

the largest FNR, to show recovery results. On CIFAR-10 dataset under Edge attack, the original global model has testing accuracy 81.9% and ASR 17.4%; and after detecting malicious clients and re-training a global model, these numbers change to 82.8% and 5.6%, respectively. Note that the server can also re-train a global model with small communication/computation cost for the clients using FedRecover [18].

7 Adaptive Attacks

Our theoretical analysis in Section 5 shows the security of FLForensics against any (adaptive) poisoning attack that satisfies the formal definition. In other words, an adaptive attack that deviates from such definition may degrade the performance of FLForensics. However, such adaptive attack may also be less effective, i.e., achieve smaller ASR. We empirically evaluate multiple such adaptive attacks. In these following experiments, FLForensics uses the default settings, e.g., CIFAR-10 dataset, 150 check points, and the server selects all clients in each training round.

Attack frequency: One adaptive attack is that each malicious client performs attacks only in some certain selected training rounds, violating the poisoning attack definition in Definition 1. In particular, when a malicious client does not perform attack in a training round, it calculates its model update based on the clean local training data. Table 11a shows the results of FLForensics when the malicious clients perform the Scaling attack in every e training rounds,

where e ranges from 1 to 10. We find that when the malicious clients perform attack every 10 or more rounds, FLForensics cannot accurately detect the malicious clients. This is because the attacks are ineffective, i.e., ASRs are less than 12%. In other words, FLForensics can accurately detect malicious clients for the adaptive attack once it is effective, i.e., attack frequently and achieve high ASRs.

Attack probability: Other than performing attacks periodically in every e training rounds, an attacker can also choose to perform attack in each training round with a certain probability. Such attack may be more stealthy and harder to trace back. Table 11b shows the results when a malicious client launches the Scaling attack with a probability p in each training round, where p ranges from 0.2 to 1.0. We observe that ASR decreases as p decreases. FLForensics accurately detects malicious clients when $p \geq 0.5$, with a FPR not exceeding 1.25%. When $p = 0.2$, the attack has an ASR of 20%. Since the attack is less effective in this scenario, FLForensics has a higher FNR at detecting malicious clients. However, FLForensics still achieves a small FPR, with at most one benign client misclassified as malicious.

Trigger location: Following [16], we place the trigger at the upper right corner of an image by default. Table 11c illustrates the performance of FLForensics when the Scaling attack places the trigger at different locations, where UR, LR, UL, and LL represent the trigger is at the upper right corner, lower right corner, upper left corner, and lower left corner of an image, respectively. Note that the trigger in these experiments is the same as that in [16]. We also evaluate adding the trigger at a random location of each image in each training round, which corresponds to the ‘Random’ row. The results show that when the trigger’s location is fixed, the attack is generally more effective, with only the UL trigger location having a lower ASR, and FLForensics can correctly identify malicious clients in such scenarios. When the attacker introduces the trigger at random locations, the attack becomes less effective, and thus FLForensics misses some malicious clients (FNR is around 30%). Our results show that FLForensics performs well across various trigger locations that achieve high ASRs. We note that previous work [34] showed that trigger location including random location does not have much impact on an attack’s ASR. We have a different observation in our experiments. This is because the previous work was for centralized learning, while our results are for FL.

Trigger value: To investigate the performance of FLForensics under different trigger values, we vary the pixel value of the trigger, where the trigger shape is from Bagdasaryan et al. [16]. Specifically, we select three different RGB values for each pixel of the trigger, i.e., (255, 255, 255), (204, 204, 204), and (0, 0, 0). Additionally, we use a random trigger, each pixel of which has random RGB values. Table 11e shows these triggers and the corresponding performance of FLForensics. Our results indicate that once the attack is effective, FLForensics can accurately trace back malicious clients. FLForensics misses all the malicious clients when the trigger value is (0, 0, 0). This is because this trigger value is ineffective at all, i.e., ASR=0.

Trigger size: Table 11d shows the results of FLForensics when the Scaling attack uses different trigger sizes, where the trigger is a white square located at the upper right corner. We observe that as the trigger size increases, ASR also increases. When the trigger size is 2×2 , the attack has almost no effect, leading to inaccurate detection of malicious clients for FLForensics. However, when the trigger size is greater than or equal to 3×3 , FLForensics can correctly identify all malicious clients, even with an ASR of only 14.2%. These results show that once the trigger size is large enough to make the attack somewhat effective, our FLForensics performs well.

Summary: Our experimental results show that once a (adaptive) poisoning attack is effective, i.e., ASR is somewhat large, FLForensics can accurately trace back the malicious clients. This leads to a dilemma for an attacker: if an attacker aims to evade FLForensics, its attack becomes less or not effective.

8 Discussion and Limitations

Detecting misclassified target input: FLForensics assumes the given misclassified input is a target input. When the misclassified input is not a target input, FLForensics cannot identify malicious clients since they may not contribute to the misclassification. We find that FLForensics can be adapted to accurately detect whether a misclassified input is a target input or not. For instance, given a misclassified input x and a non-target input x' , we calculate the influence

Table 12: Results of FLForensics when using a random or true input as a non-target input.

Dataset	Non-target input	Scaling attack			ALIE attack			Edge attack		
		DACC	FPR	FNR	DACC	FPR	FNR	DACC	FPR	FNR
CIFAR-10	Random	1.000	0.000	0.000	1.000	0.000	0.000	0.980	0.000	0.100
	True	1.000	0.000	0.000	1.000	0.000	0.000	0.970	0.013	0.100
Fashion-MNIST	Random	1.000	0.000	0.000	1.000	0.000	0.000	1.000	0.000	0.000
	True	1.000	0.000	0.000	1.000	0.000	0.000	1.000	0.000	0.000
MNIST	Random	1.000	0.000	0.000	1.000	0.000	0.000	1.000	0.000	0.000
	True	1.000	0.000	0.000	1.000	0.000	0.000	1.000	0.000	0.000
Sentiment140	Random	0.980	0.025	0.000	1.000	0.000	0.000	0.970	0.038	0.000
	True	0.990	0.013	0.000	1.000	0.000	0.000	0.990	0.013	0.000
ImageNet-Fruits	Random	1.000	0.000	0.000	1.000	0.000	0.000	0.950	0.031	0.125
	True	1.000	0.000	0.000	1.000	0.000	0.000	0.950	0.031	0.125

scores (s_i, s'_i) for all clients and obtain potential malicious clusters using Algorithm 1. Our intuition is that if every potential malicious cluster has similar average s_i and s'_i , which means that we cannot distinguish between x and x' with respect to their influences, we detect that the misclassified input x is a non-target input. Specifically, if every potential malicious cluster c_{p_j} satisfies $\alpha \leq \sum_{i \in c_{p_j}} s'_i / \sum_{i \in c_{p_j}} s_i \leq \frac{1}{\alpha}$ for some $\alpha < 1$, we detect x as a non-target input, otherwise we detect it as a target input. To evaluate the effectiveness of the above method, we randomly pick 50 misclassified target inputs and 50 misclassified non-target inputs. We set $\alpha = 0.2$. We find that our method can effectively distinguish between target and non-target inputs, i.e., our method correctly classifies 96% of target inputs and 98% of non-target inputs.

Table 13: Impact of different aggregation rules on FLForensics under ALIE and Edge attacks. The results for the Scaling attack are shown in Table 8.

Aggregation	ALIE attack			Edge attack		
	DACC	FPR	FNR	DACC	FPR	FNR
Trim	1.000	0.000	0.000	0.980	0.000	0.100
Median	1.000	0.000	0.000	0.980	0.000	0.100
FLTrust	1.000	0.000	0.000	0.980	0.000	0.100
FLAME	1.000	0.000	0.000	0.920	0.100	0.000

Using true input as non-target input: In our experiments, we use a random input (e.g., a random image) as a non-target input in FLForensics. When a true input with the target label is available, the server can also use it as the non-target input. Table 12 compares the results when FLForensics uses a random input or true input as the non-target input on the five datasets and three attacks. We find that random inputs and true inputs achieve comparable results in most cases, except several cases, for which true inputs achieve slightly lower FPRs. These results indicate that if a true input with the target label from the learning task’s data distribution is available, the server can use it as the non-target input.

Forensics for clean-label targeted attacks: We focus on tracing back dirty-label attacks in this work, where the poisoned training examples have the same label as the target label. We find that for clean-label attacks, where only the training data is poisoned without changing their labels, FLForensics can still effectively trace back the malicious clients. This is because it leverages clients’ model updates instead of their local training data. Once the model updates are backdoored, FLForensics can trace back. Furthermore, we test FLForensics on clean-label attack [35] using CIFAR-10 and FedAvg. We train ‘cat’ images to have feature vectors similar to ‘dog’ images, while keeping their ‘cat’ labels. Under our default experimental settings, the DACC, FPR, and FNR are respectively 0.95, 0.0625, and 0.0, demonstrating the effectiveness of FLForensics.

Table 14: Results for centralized learning.

Method	DACC	FPR	FNR
PF	0.831	0.189	0.000
FLForensics-G	0.828	0.191	0.000
FLForensics-A	0.826	0.194	0.000
FLForensics	0.992	0.008	0.005
FLForensics-True	0.998	0.002	0.000

Forensics for untargeted poisoning attacks: In this work, we focus on forensics for targeted poisoning attacks. An interesting future work is to extend our FLForensics to untargeted poisoning attacks [4]. In untargeted poisoning attacks, a poisoned global model makes incorrect predictions for indiscriminate clean testing inputs, leading to a low testing accuracy. For instance, we found that the current FLForensics is ineffective at detecting malicious clients when given a misclassified input in an untargeted poisoning attack [4] and a non-target input. This is because the misclassified input in an untargeted poisoning attack is also a non-target input.

Extending FLForensics to centralized learning: Our FLForensics can also be extended to centralized learning. In particular, we treat a training example as a “client”; w_t in Equation 5 and 6 is the model in the t th mini-batch when training a model; and $g_t^{(i)}$ is the gradient of the cross-entropy loss of w_t for the i th training example. We find that when the training dataset is unbalanced (i.e., like non-iid in FL) and the target label is a class that has more training examples, FLForensics substantially outperforms existing poison-forensics methods for centralized learning. For instance, Table 14 shows the results for different methods at tracing back the poisoned training examples, where FLForensics-True means using a true input as the non-target input. The dataset is sampled from CIFAR-10, where Figure 5 in Appendix shows the distribution of training examples among the classes in our experiments. We performed a targeted poisoning attack to the dataset: the target label is 1; and we inject the trigger used in our FL experiments into 10% of the training inputs.

Extra privacy concerns of storing checkpoints: FLForensics requires the server to save checkpoints during training process in order to trace back malicious clients. These checkpoints include the global model parameters and clients’ local model updates. Therefore, it is worth discussing the potential privacy concerns associated with storing these information. In Section 3, we assume that the server is not compromised by an attacker. Under this threat model, storing checkpoints on the server does not pose any extra privacy issues. However, if there is a risk of server compromise, the additional privacy concerns introduced by storing checkpoints depend on whether the server is compromised and when the compromise occurs. If the server is compromised before the training starts, the attacker can easily access and save the checkpoints, and thus storing them would not introduce additional privacy concerns. On the other hand, if the server is compromised after training, we acknowledge that storing checkpoints may raise extra privacy concerns since the attacker can access them.

9 Conclusion and Future Work

In this work, we propose FLForensics, the first poison-forensics method to trace back malicious clients in FL. We theoretically show the security of FLForensics against (adaptive) poisoning attacks under a formal definition of poisoning attack. Moreover, our empirical evaluation results on multiple benchmark datasets show that FLForensics can accurately trace back malicious clients against both state-of-the-art and adaptive poisoning attacks. An interesting future work is to extend FLForensics to untargeted poisoning attacks and explore the security of FLForensics against strategically crafted misclassified target input.

References

- [1] B. McMahan, E. Moore, D. Ramage, S. Hampson, and B. A. y Arcas, "Communication-efficient learning of deep networks from decentralized data," in *AISTATS*, 2017.
- [2] *Utilization of FATE in Risk Management of Credit in Small and Micro Enterprises*. [Online]. Available: <https://www.fedai.org/cases/utilization-of-fate-in-risk-management-of-credit-in-small-and-micro-enterprises/>
- [3] *Federated Learning: Collaborative Machine Learning without Centralized Training Data*. [Online]. Available: <https://ai.googleblog.com/2017/04/federated-learning-collaborative.html>
- [4] M. Fang, X. Cao, J. Jia, and N. Gong, "Local model poisoning attacks to byzantine-robust federated learning," in *USENIX Security Symposium*, 2020.
- [5] M. Baruch, G. Baruch, and Y. Goldberg, "A little is enough: Circumventing defenses for distributed learning," in *NeurIPS*, 2019.
- [6] H. Wang, K. Sreenivasan, S. Rajput, H. Vishwakarma, S. Agarwal, J.-y. Sohn, K. Lee, and D. Papailiopoulos, "Attack of the tails: Yes, you really can backdoor federated learning," in *NeurIPS*, 2020.
- [7] D. Yin, Y. Chen, R. Kannan, and P. Bartlett, "Byzantine-robust distributed learning: Towards optimal statistical rates," in *ICML*, 2018.
- [8] T. D. Nguyen, P. Rieger, H. Chen, H. Yalame, H. Möllering, H. Fereidooni, S. Marchal, M. Miettinen, A. Mirhoseini, S. Zeitouni *et al.*, "Flame: Taming backdoors in federated learning," in *USENIX Security Symposium*, 2022.
- [9] X. Cao, M. Fang, J. Liu, and N. Z. Gong, "Fltrust: Byzantine-robust federated learning via trust bootstrapping," in *NDSS*, 2021.
- [10] X. Cao, J. Jia, and N. Z. Gong, "Provably secure federated learning against malicious clients," in *AAAI*, 2021.
- [11] Z. Zhang, X. Cao, J. Jia, and N. Z. Gong, "Fldetector: Defending federated learning against model poisoning attacks via detecting malicious clients," in *KDD*, 2022.
- [12] Y. Gao, C. Xu, D. Wang, S. Chen, D. C. Ranasinghe, and S. Nepal, "Strip: A defence against trojan attacks on deep neural networks," in *ACSAC*, 2019.
- [13] E. Chou, F. Tramer, and G. Pellegrino, "Sentinet: Detecting localized universal attacks against deep learning systems," in *S&P Workshops*, 2020.
- [14] W. Ma, D. Wang, R. Sun, M. Xue, S. Wen, and Y. Xiang, "The "beatrice" resurrections: Robust backdoor detection via gram matrices," in *NDSS*, 2023.
- [15] R. J. Campello, D. Moulavi, and J. Sander, "Density-based clustering based on hierarchical density estimates," in *PAKDD*, 2013.
- [16] E. Bagdasaryan, A. Veit, Y. Hua, D. Estrin, and V. Shmatikov, "How to backdoor federated learning," in *AISTATS*, 2020.
- [17] X. Cao, Z. Zhang, J. Jia, and N. Z. Gong, "Flcert: Provably secure federated learning against poisoning attacks," in *IEEE Transactions on Information Forensics and Security*, 2022.

- [18] X. Cao, J. Jia, Z. Zhang, and N. Z. Gong, “Fedrecover: Recovering from poisoning attacks in federated learning using historical information,” in *IEEE Symposium on Security and Privacy*, 2023.
- [19] S. Shan, A. N. Bhagoji, H. Zheng, and B. Y. Zhao, “Poison forensics: Traceback of data poisoning attacks in neural networks,” in *USENIX Security Symposium*, 2022.
- [20] Z. Hammoudeh and D. Lowd, “Identifying a training-set attack’s target using renormalized influence estimation,” in *CCS*, 2022.
- [21] S. Cheng, G. Tao, Y. Liu, S. An, X. Xu, S. Feng, G. Shen, K. Zhang, Q. Xu, S. Ma *et al.*, “Beagle: Forensics of deep learning backdoor attack for better defense,” in *NDSS*, 2023.
- [22] S. Boyd, S. P. Boyd, and L. Vandenberghe, *Convex optimization*. Cambridge university press, 2004.
- [23] H. Xiong, “Dpcd: Discrete principal coordinate descent for binary variable problems,” in *AAAI*, 2022.
- [24] A. Krizhevsky, G. Hinton *et al.*, “Learning multiple layers of features from tiny images,” 2009.
- [25] H. Xiao, K. Rasul, and R. Vollgraf. (2017) Fashion-mnist: a novel image dataset for benchmarking machine learning algorithms.
- [26] Y. LeCun, C. Cortes, and C. Burges, “Mnist handwritten digit database,” Available: [http://yann. lecun. com/exdb/mnist](http://yann.lecun.com/exdb/mnist), 1998.
- [27] A. Go, R. Bhayani, and L. Huang, “Twitter sentiment classification using distant supervision,” *CS224N project report, Stanford*, 2009.
- [28] G. Cazenavette, T. Wang, A. Torralba, A. A. Efros, and J.-Y. Zhu, “Dataset distillation by matching training trajectories,” in *CVPR*, 2022.
- [29] J. Deng, W. Dong, R. Socher, L.-J. Li, K. Li, and L. Fei-Fei, “Imagenet: A large-scale hierarchical image database,” in *CVPR*, 2009.
- [30] K. He, X. Zhang, S. Ren, and J. Sun, “Deep residual learning for image recognition,” in *CVPR*, 2016.
- [31] S. Hochreiter and J. Schmidhuber, “Long short-term memory,” in *Neural computation*, 1997.
- [32] T. Gu, B. Dolan-Gavitt, and S. Garg, “Badnets: Identifying vulnerabilities in the machine learning model supply chain,” in *IEEE Access*, 2019.
- [33] F. Ripening, “Banana ripening process dataset,” <https://universe.roboflow.com/fruit-ripening/banana-ripening-process>. [Online]. Available: <https://universe.roboflow.com/fruit-ripening/banana-ripening-process>
- [34] A. Salem, R. Wen, M. Backes, S. Ma, and Y. Zhang, “Dynamic backdoor attacks against machine learning models,” in *EuroS&P*, 2022.
- [35] A. Shafahi, W. R. Huang, M. Najibi, O. Suci, C. Studer, T. Dumitras, and T. Goldstein, “Poison frogs! targeted clean-label poisoning attacks on neural networks,” in *NeurIPS*, 2018.

A Appendix

A.1 Proof of Theorem 1

By setting $\delta = g_t^{(i)}$ in Assumption 1, we have the following for each check-point training round t :

$$\begin{aligned}\ell_{CE}(x, y; w_t + g_t^{(i)}) &= \ell_{CE}(x, y; w_t) \\ &\quad + \nabla \ell_{CE}(x, y; w_t)^\top g_t^{(i)}.\end{aligned}\tag{13}$$

Similarly, by setting $\delta = g_t^{(j)}$ in Assumption 1, we have:

$$\begin{aligned}\ell_{CE}(x, y; w_t + g_t^{(j)}) &= \ell_{CE}(x, y; w_t) \\ &\quad + \nabla \ell_{CE}(x, y; w_t)^\top g_t^{(j)}.\end{aligned}\tag{14}$$

By combining Equation 8, 13, and 14, we have:

$$\nabla \ell_{CE}(x, y; w_t)^\top g_t^{(i)} \leq \nabla \ell_{CE}(x, y; w_t)^\top g_t^{(j)}.\tag{15}$$

Since the learning rate $\alpha_t > 0$ and $C_t = \{1, 2, \dots, n\}$ in each check-point training round, we have the following by summing over the check-point training rounds on both sides of Equation 15:

$$\sum_{t \in \Omega} \alpha_t \nabla \ell_{CE}(x, y; w_t)^\top g_t^{(i)} \leq \sum_{t \in \Omega} \alpha_t \nabla \ell_{CE}(x, y; w_t)^\top g_t^{(j)}\tag{16}$$

$$\iff -s_i \leq -s_j.\tag{17}$$

Therefore, we have Equation 10, which completes the proof.

A.2 Proof of Theorem 2

According to Assumption 2, we have:

$$\ell_{CE}(x, y; w_t + g_t^{(j_1)}) \leq \ell_{CE}(x, y; w_t + g_t^{(j_2)}).\tag{18}$$

By setting $\delta = g_t^{(j_1)}$ and $\delta = g_t^{(j_2)}$ in Assumption 1, we can get:

$$\begin{aligned}\ell_{CE}(x, y; w_t + g_t^{(j_1)}) &= \ell_{CE}(x, y; w_t) \\ &\quad + \nabla \ell_{CE}(x, y; w_t)^\top g_t^{(j_1)},\end{aligned}\tag{19}$$

$$\begin{aligned}\ell_{CE}(x, y; w_t + g_t^{(j_2)}) &= \ell_{CE}(x, y; w_t) \\ &\quad + \nabla \ell_{CE}(x, y; w_t)^\top g_t^{(j_2)}.\end{aligned}\tag{20}$$

By combining Equation 18, 19, and 20, we have:

$$\nabla \ell_{CE}(x, y; w_t)^\top g_t^{(j_1)} \leq \nabla \ell_{CE}(x, y; w_t)^\top g_t^{(j_2)}.\tag{21}$$

Since the learning rate $\alpha_t > 0$ and $C_t = \{1, 2, \dots, n\}$ in each check-point training round, we have the following by summing over the check-point training rounds on both sides of Equation 21:

$$\sum_{t \in \Omega} \alpha_t \nabla \ell_{CE}(x, y; w_t)^\top g_t^{(j_1)} \leq \sum_{t \in \Omega} \alpha_t \nabla \ell_{CE}(x, y; w_t)^\top g_t^{(j_2)}\tag{22}$$

$$\iff -s_{j_1} \leq -s_{j_2},\tag{23}$$

which gives Equation 11 and completes the proof.

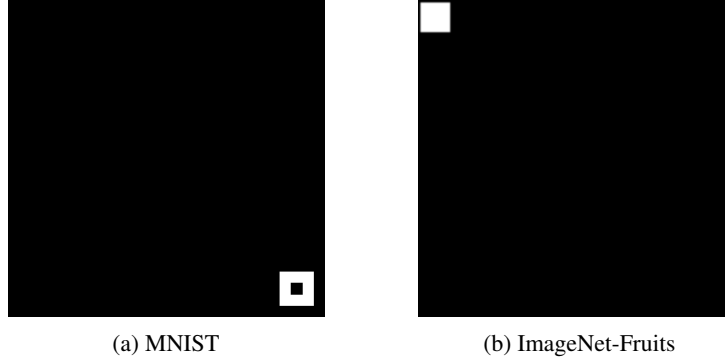


Figure 4: Triggers in MNIST and ImageNet-Fruits datasets.

A.3 Proof of Theorem 3

By setting $\delta = g_t^{(i)}$ in Assumption 1, we have the following for each check-point training round t :

$$\begin{aligned} \ell_{CE}(x', y; w_t + g_t^{(i)}) &= \ell_{CE}(x', y; w_t) \\ &\quad + \nabla \ell_{CE}(x', y; w_t)^\top g_t^{(i)}. \end{aligned} \quad (24)$$

Similarly, by setting $\delta = g_t^{(j)}$ in Assumption 1, we have:

$$\begin{aligned} \ell_{CE}(x', y; w_t + g_t^{(j)}) &= \ell_{CE}(x', y; w_t) \\ &\quad + \nabla \ell_{CE}(x', y; w_t)^\top g_t^{(j)}. \end{aligned} \quad (25)$$

By combining Equation 7, 24, and 25, we have:

$$\nabla \ell_{CE}(x', y; w_t)^\top g_t^{(i)} \geq \nabla \ell_{CE}(x', y; w_t)^\top g_t^{(j)}. \quad (26)$$

Since the learning rate $\alpha_t > 0$ and $C_t = \{1, 2, \dots, n\}$ in each check-point training round, we have the following by summing over the check-point training rounds on both sides of Equation 26:

$$\sum_{t \in \Omega} \alpha_t \nabla \ell_{CE}(x', y; w_t)^\top g_t^{(i)} \geq \sum_{t \in \Omega} \alpha_t \nabla \ell_{CE}(x', y; w_t)^\top g_t^{(j)} \quad (27)$$

$$\iff -s'_i \geq -s'_j. \quad (28)$$

By combining Equations 17 and 28, we have Equation 12, which completes the proof.

A.4 Proof of Corollary 1

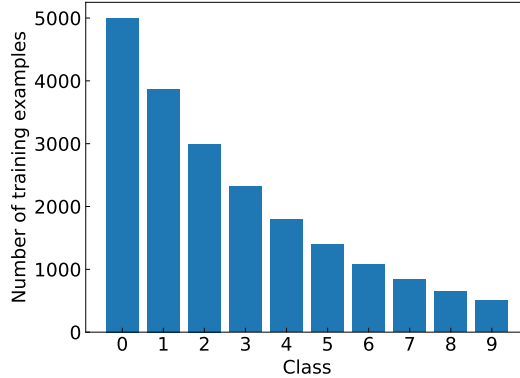
From Equation 17 and Equation 28, we have $s'_i \leq s'_j$ and $s_i \geq s_j$. Since $s_i > 0$ and $s_j > 0$, we have:

$$\frac{s'_i}{s_i} \leq \frac{s'_j}{s_j}, \quad (29)$$

which completes the proof.

Table 15: CNN architecture for Fashion-MNIST and MNIST.

Layer	Size
Input	$28 \times 28 \times 1$
Convolution + ReLU	$3 \times 3 \times 30$
Max Pooling	2×2
Convolution + ReLU	$3 \times 3 \times 50$
Max Pooling	2×2
Fully Connected + ReLU	100
Softmax	10

**Figure 5: Number of training examples for each class, where class distribution is roughly a power-law. We sample the unbalanced dataset from CIFAR-10. We have 20,431 training examples in total.****Table 16: Default parameter setting. Since ImageNet-Fruits only has 40 clients and 8 malicious clients, and “min_cluster_size” is set to 7, when performing clustering using HDBSCAN, we duplicate the influence scores of all clients before clustering, resulting in a total of 80 influence scores.**

Parameter	CIFAR-10	Fashion-MNIST	MNIST	Sentiment140	ImageNet-Fruits
# clients	100			40	
# malicious clients	20			8	
# rounds	1500	2000	2000	1500	1000
# local training epochs	1				
Batch size	64	32	32	32	64
Learning rate	1×10^{-2}	6×10^{-3}	3×10^{-4}	1×10^{-1} (decay at the 800th epoch with factor 0.5)	1×10^{-2}
# check points	150	200	200	150	100
min_cluster_size	7				

A.5 Extending GAS to FL

Since the total number of training examples possessed by all clients is much larger than the number of clients, when we detect malicious training examples, we use HDBSCAN to divide the examples into a big cluster (size is at least half of the whole training dataset size) and *outliers* with respect to their influence scores by setting “min_cluster_size” as $|D|/2 + 1$, where $|D|$ is the whole training dataset size. Unlike FLForensics, we adopt the Euclidean distance metric for HDBSCAN since GAS only has one-dimensional influence score, for which scaling is meaningless. We then use the outliers to determine the threshold since the big cluster corresponds to the majority clean training examples. Specifically, HDBSCAN outputs a *confidence level* (a number between 0 and 1) for each outlier, which indicates the confidence HDBSCAN has at predicting an input as outlier. We adopt a confidence level of 95%, which is widely used in statistics. Specifically, we treat the outliers whose confidence levels are at least 95% and whose influence scores are positive as “true” outliers. Moreover, we set the smallest influence score of such true outliers as the threshold.

Table 17: Results of PF and FLForensics-G when they use the clients’ model updates.

Method	Scaling attack			ALIE attack			Edge attack		
	DACC	FPR	FNR	DACC	FPR	FNR	DACC	FPR	FNR
PF	0.900	0.125	0.000	0.900	0.125	0.000	0.920	0.100	0.000
FLForensics-G	0.850	0.150	0.150	0.880	0.150	0.000	0.880	0.138	0.050

A.6 Simulating Non-iid Setting in FL

Following previous works [4, 9], to simulate the non-iid data distribution across clients, we randomly partition all clients into C groups, where C is the number of classes. We then assign each training example with label y to the clients in one of these C groups with a probability. In particular, a training example with label y is assigned to clients in group y with a probability of ρ , and to clients in any other groups with an equal probability of $\frac{1-\rho}{C-1}$, where $\rho \in [0.1, 1.0]$. Within the same group, the training example is uniformly distributed among the clients. Therefore, ρ controls the degree of non-iid. When $\rho = 0.1$, the local training data follows an iid distribution in our datasets; otherwise, the clients’ local training data is non-iid. A higher value ρ implies a higher degree of non-iid.

Table 18: Test accuracy (TACC) and attack success rate (ASR) of different FL aggregation rules under different attacks. For the Trim aggregation rule, the trim parameter is set to the number of malicious clients. The server in FLTrust holds a small and clean root dataset. In our experiments, the size of the root dataset is set to 50, and the root dataset is drawn from the same distribution as that of the learning task’s overall training data. For the FLAME aggregation rule, we use the same parameters as in [8]. We do not show ASR when there is no attack (i.e., “—”) because different attacks use different triggers.

(a) CIFAR-10

Attack	FedAvg		Trim		Median		FLTrust		FLAME	
	TACC	ASR	TACC	ASR	TACC	ASR	TACC	ASR	TACC	ASR
No attack	0.837	—	0.769	—	0.755	—	0.811	—	0.774	—
Scaling attack	0.831	0.682	0.777	0.950	0.780	0.930	0.816	0.642	0.776	0.644
ALIE attack	0.843	0.956	0.814	0.754	0.809	0.980	0.806	0.968	0.780	0.958
Edge attack	0.819	0.174	0.761	0.337	0.762	0.352	0.794	0.056	0.789	0.087

(b) Fashion-MNIST

Attack	FedAvg		Trim		Median		FLTrust		FLAME	
	TACC	ASR	TACC	ASR	TACC	ASR	TACC	ASR	TACC	ASR
No attack	0.900	—	0.856	—	0.864	—	0.880	—	0.887	—
Scaling attack	0.887	0.953	0.870	0.892	0.841	0.043	0.874	0.037	0.890	0.024
ALIE attack	0.889	0.941	0.809	0.113	0.764	0.040	0.876	0.038	0.886	0.020
Edge attack	0.886	0.990	0.862	1.000	0.856	1.000	0.861	0.990	0.883	0.990

(c) MNIST

Attack	FedAvg		Trim		Median		FLTrust		FLAME	
	TACC	ASR	TACC	ASR	TACC	ASR	TACC	ASR	TACC	ASR
No attack	0.960	—	0.948	—	0.943	—	0.926	—	0.948	—
Scaling attack	0.958	0.950	0.921	0.013	0.936	0.010	0.926	0.006	0.954	0.005
ALIE attack	0.958	0.944	0.788	0.045	0.929	0.013	0.927	0.007	0.953	0.005
Edge attack	0.953	0.990	0.938	0.980	0.939	0.960	0.919	0.580	0.953	0.070

(d) SENT140

Attack	FedAvg		Trim		Median		FLTrust		FLAME	
	TACC	ASR	TACC	ASR	TACC	ASR	TACC	ASR	TACC	ASR
No attack	0.660	—	0.684	—	0.673	—	0.494	—	0.589	—
Scaling attack	0.659	0.995	0.616	0.985	0.645	1.000	0.494	1.000	0.592	0.232
ALIE attack	0.687	1.000	0.654	1.000	0.531	0.801	0.494	1.000	0.651	0.122
Edge attack	0.564	0.600	0.567	0.683	0.609	0.858	0.494	1.000	0.581	0.175

(e) ImageNet-fruits

Attack	FedAvg		Trim		Median		FLTrust		FLAME	
	TACC	ASR	TACC	ASR	TACC	ASR	TACC	ASR	TACC	ASR
No attack	0.517	—	0.537	—	0.509	—	0.480	—	0.492	—
Scaling attack	0.494	0.881	0.465	0.749	0.467	0.842	0.473	0.108	0.494	0.102
ALIE attack	0.488	1.000	0.486	0.113	0.469	0.132	0.482	0.115	0.502	0.952
Edge attack	0.514	0.283	0.529	0.279	0.502	0.219	0.490	0.377	0.470	0.465